Chinese Chemical Letters 35 (2024) 108636

Contents lists available at ScienceDirect

Chinese Chemical Letters

journal homepage: www.elsevier.com/locate/cclet

Ultrastable graphene isolated AuAg nanoalloy for SERS biosensing and photothermal therapy of bacterial infection

Shengkai Li[a,b], Zhiyang Li[a], Qing Hao[a], Shen Wang[a], Yanxia Yang[a], Jieqiong Xu[a], Zhiwei Yin[a], Liang Zhang[a], Zhuo Chen[a,*]

[a] *Molecular Science and Biomedicine Laboratory (MBL), State Key Laboratory of Chemo/Biosensing and Chemometrics, College of Chemistry and Chemical Engineering, College of Biology, Aptamer Engineering Center of Hunan Province, Hunan University, Changsha 410082, China*
[b] *School of Chemistry and Chemical Engineering/Guangzhou Key Laboratory for Clean Energy and Materials/Key Laboratory for Water Quality and Conservation of the Pearl River Delta, Ministry of Education, Guangzhou University, Guangzhou 510006, China*

ARTICLE INFO

Article history:
Received 12 February 2023
Revised 4 May 2023
Accepted 31 May 2023
Available online 2 June 2023

Keywords:
Localized surface plasmon resonance
Graphitic shell isolated AuAg nanoalloy (GAA)
Surface–enhanced Raman scattering (SERS)
Bacterial biomarker detection
Photothermal antibacterial therapy

ABSTRACT

Plasmonic metal nanomaterials with intrinsic surface–enhanced Raman scattering (SERS) and photothermal properties, especially AuAg nanoalloys with both the outstanding merits of Au and Ag nanocrystals, show huge application prospects in bacterial theranostics. However, the direct exposure of AuAg nanoalloys in external conditions probably cause undesirable reactions and poisonous metal ion leakage during SERS detection and photothermal antibacterial therapy process, which severely hinder bacterial theranostics applications. Herein, we report an ultrastable graphene–isolated AuAg nanoalloy (GAA) with AuAg core confined in few–layer graphitic shell as a versatile platform for bacterial detection and therapy. The encapsulation of graphene ensures the good stability of AuAg core, that its superior SERS and photothermal properties are therefore further guaranteed. GAA is used for SERS detection of two vital bacterial biomarkers (including corrosive cyanide and pyocyanin), exhibiting good SERS quantitative and multiplexing ability. GAA is further used for photothermal antibacterial therapy application, and ultrahigh antibacterial efficacies for both Gram–negative *Escherichia coli* and Gram–positive *Staphylococcus aureus* are achieved under 808 nm laser irradiation. This work proposes a valuable method to develop robust bacterial theranostic platform.

High morbidity and mortality caused by bacterial infection has become a major threat to human beings [1–3], thus robust platform is urgently required for bacterial detection and therapy. Plasmonic metal nanomaterials with superior surface–enhanced Raman scattering (SERS) and photothermal properties are reported to have great application potential in bacterial theranostics [4–6]. SERS technique not only provides rich molecular fingerprint information, but also shows ultralow detection limit down to single molecule level, resistance to photodegradation and photobleaching as well as low background interference, it is therefore suited for bioanalysis [7–9]. Photothermal therapy (PTT) strategy, especially the near infrared (NIR) light mediated photothermal antibacterial therapy with the merits of acceptable controllability, high tissue penetration and minor tissue trauma, is considered as one of the most promising next–generation antibacterial strategies [10–12].

Au and Ag nanocrystals (NCs) are the most widely used plasmonic metal nanomaterials [13,14]. Au NCs with satisfactory chemical stability and tunable optical absorption in NIR region, show immense promise in photothermal antibacterial applications, but they are expensive and have relative lower SERS activity than Ag NCs. As compared, Ag NCs have more extensive applications in SERS bioanalysis theoretically because of their larger optical absorption cross section and lower cost, but they are highly sensitive to oxidation environments and their optical absorption is commonly within ultraviolet–visible (UV–vis) region [15,16]. It is thus reasonable to infer that AuAg nanoalloy containing both Au and Ag particle domains show much greater application prospects in SERS detection and PTT of bacterial infection. However, AuAg nanoalloy probably exhibits poor stability in some harsh conditions like *Pseudomonas aeruginosa* (*P. aeruginosa*) infection environment rich in corrosive cyanide (CN^-) [17] and hyperthermia environment [18]. Also, the direct exposure of AuAg nanoalloy in external conditions is bound to cause side reactions and poisonous metal ion leakage during SERS detection and photothermal antibacterial therapy process [19,20]. Hence, it is highly non–trivial to prevent AuAg nanoal-

* Corresponding author.
E-mail address: zhuochen@hnu.edu.cn (Z. Chen).

https://doi.org/10.1016/j.cclet.2023.108636
1001-8417/

loy from complex environments for more reliable SERS bioanalysis and effective photothermal antibacterial therapy.

Graphene with excellent stability is considered to be a desirable isolation material to prevent plasmonic metal nanomaterials from dissolution and agglomeration, and meanwhile without significantly affecting their inherent properties [21,22]. Especially, it is able to quench the background fluorescence interference and avoid undesired reactions catalyzed by metal core during the SERS detection process, and its broad–spectrum absorption characteristic is beneficial to improve the photothermal property of plasmonic nanomaterials [19–22]. In this work, we applied the chemical vapor deposition (CVD) method to prepare ultrastable graphitic shell isolated AuAg nanoalloy (GAA) as a versatile platform for SERS detection and PTT of bacterial infection. GAA with optimized SERS property and superior stability was obtained *via* rational modulation of experimental parameters. Subsequent studies proved the GAA had excellent stability in high concentration of H_2O_2, NaHS and HNO_3 solution, indicative of its satisfactory corrosion resistance. Also, its superior NIR laser mediated photothermal heating capacity was also proved. On that basis, GAA was firstly used as a robust SERS substrate for the detection of two vital biomarkers in *P. aeruginosa* infection, including corrosive CN^- and pyocyanin (PYO), and the results illustrated its good SERS quantitative and multiplexing ability. GAA was further used as a photothermal reagent for NIR light mediated photothermal antibacterial applications, and ultrahigh antibacterial efficiencies for Gram–negative *Escherichia coli* (*E. coli*) and Gram–positive *Staphylococcus aureus* (*S. aureus*) were achieved under 808 nm laser irradiation. We expected the versatile and ultrastable GAA platform could be a robust tool for bacterial theranostics in future clinical trials.

Ultrastable GAA with AuAg nanoalloy confined in few–layer graphitic shell was prepared by the CVD method [19,22]. The procedure and possible mechanism for GAA preparation were showed in Fig. 1a. Concretely, the Au and Ag precursors confined in the fumed SiO_2 template firstly became AuAg alloy nanodroplets *via* H_2 reduction under high temperature, then the saturated carbon atoms from CH_4 cracking were dissolved and deposited on AuAg alloy surface. Finally, graphene was encapsulated on AuAg surface to form GAA.

To achieve both superior SERS property and stability, Au/Ag ratio and CH_4 supply time were systematically optimized. At first, 8 groups of GAAs with different Au/Ag mass ratios (groups 1–8: ~1: 0.3, 0.9, 1.5, 2.3, 3.1, 3.5, 3.7 and 4.1, respectively) were prepared through adjusting the input amount of Ag precursor in preparing the metal catalyst, while CH_4/H_2 flow rate and CH_4 supply time were fixed at 160/10 cm^3/min and 6 min, respectively (Fig. S1a in Supporting information). Transmission electron microscope (TEM) showed that they were all spherical and had similar particle sizes. The localized surface plasmon resonance (LSPR) absorption peak of GAA gradually blue–shifted with the increasing of Ag content, while there was almost no obvious difference in groups 6–8 (Fig. S1b in Supporting information). The results in Fig. S1c (Supporting information) showed all 8 groups of GAAs could resist the etching of 100 mmol/L H_2O_2, indicating the current CH_4/H_2 flow rate and supply time was suitable for GAA synthesis. We further used crystal violet (CV, 1 μmol/L) as the model analyte, and compared the SERS performances of different GAAs. As shown in Fig. S1d (Supporting information), the SERS signals of CV gradually augmented from groups 1–5, but that in groups 6, 7 and 8 were not significantly different. Vital information for Au/Ag ratio optimization was listed in Fig. 1b, and the conditions for the preparation of GAA in group 6 were used as the reference for further studies.

Next, we further explored the CH_4 supply time on the performance of GAA when the input amount of Ag precursor and CH_4/H_2 flow rate were fixed. As shown in the TEM images in Fig. S2a (Supporting information), the CH_4 supply time of GAA < 6 min tended to aggregation, while that ≥ 6 min had better dispersion and more uniform particle size. Also, the CH_4 supply time of GAA ≥ 6 min could resist the etching of 100 mmol/L H_2O_2 (Fig. S2b in Supporting information). We further used 1 μmol/L CV as the model analyte, the SERS performance of different GAAs with CH_4 supply time of 6, 7 and 8 min were compared. As shown in Fig. S2c (Supporting information), the SERS signal of CV decreased significantly with the increment of CH_4 supply time, which was probably be-

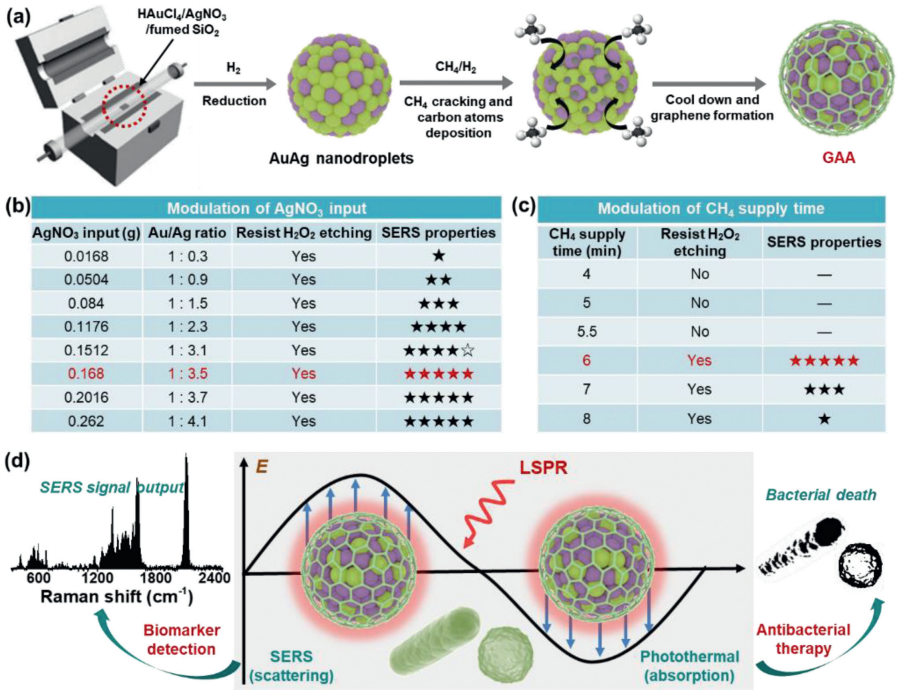

Fig. 1. Preparation and applications of GAA. (a) Procedure and mechanism of GAA synthesis *via* the CVD method. Results for optimized preparation of GAA *via* modulation of (b) Au/Ag ratio and (c) CH_4 supply time. (d) GAA used for SERS detection of bacterial biomarker and photothermal antibacterial therapy.

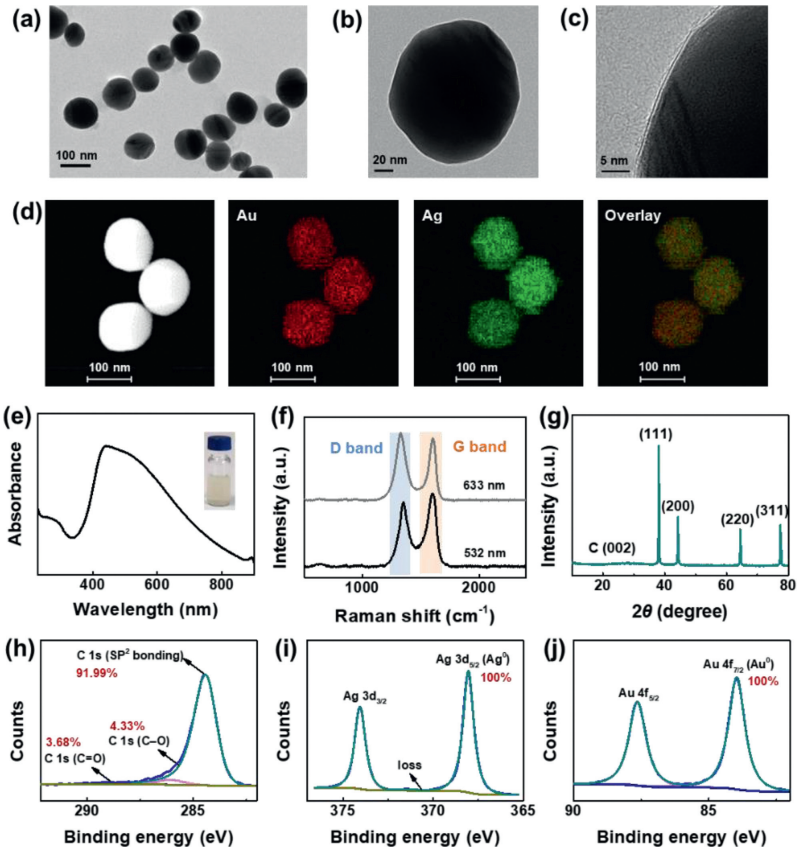

Fig. 2. Characterization of GAA. (a) TEM, (b, c) high–resolution TEM (HR–TEM) and (d) TEM/EDS elemental mapping, (e) UV–vis absorption spectrum (Inset: photo of GAA aqueous solution), (f) Raman spectra, (g) XRD spectrum and (h–j) C 1s, Ag 3d and Au 4f XPS spectra of GAA.

cause the increased thickness of graphitic shell weakened the SERS performance of AuAg nanocore. Hence, $AgNO_3$ input amount of 0.1680 g, CH_4/H_2 flow rate of 160/10 cm^3 min^{-1} and CH_4 supply time of 6 min were used for GAA preparation, and the main information for CH_4 supply time optimization was listed in Fig. 1c. The resultant GAA was expected to have both superior SERS and near–infrared (NIR) laser mediated photothermal properties, and used as a versatile platform for SERS detection of bacterial biomarker and photothermal antibacterial applications (Fig. 1d).

As shown in Fig. 2a, the GAA showed spherical and its average particle size was ~100 nm. The GAA surface was completely encapsulated with few–layer graphene (Figs. 2b and c), Au and Ag elements were evenly distributed in the AuAg nanoalloy (Fig. 2d). UV–vis absorption spectroscopy characterization indicated the light yellow colored GAA had a strong LSPR absorption peak at ~441 nm from AuAg nanoalloy and a weak absorption peak at ~265 nm from graphitic shell (Fig. 2e), and its hydrated particle size and zeta potential were 141.8 nm and −13.4 mV, respectively (Fig. S3 in Supporting information). D, G bands from graphitic shell at 1345 cm^{-1} and 1600 cm^{-1} were observed in Fig. 2f under the excitation of both 532 and 633 nm laser. We further studied the structural information of GAA in detail. As shown in the X–ray diffraction (XRD) spectrum of GAA in Fig. 2g, four strong and sharp diffraction peaks at ~38.17°, 44.37°, 64.60° and 77.52° from 111, 200, 220 and 311 crystal planes of AuAg nanoalloy were observed, respectively, indicative of its high crystallinity. [23,24] However, the diffraction peak at ~24.64° from 002 crystal plane of graphitic shell [25,26] was weak and flat, which was probably attributed to the small amount of graphene in GAA (Fig. 2g and Fig. S4 in Supporting information). X–ray photoelectron spectroscopy (XPS) tests were also used for further studying the structural information. The band at 284.48 eV belonged to the sp^2 hybridization of graphene [27], and the existence of C–O and C=O vibration indicated the graphitic shell had some defects (Fig. 2h) [28,29]. The bands at 374.08 and 368.14 eV were assigned to the Ag $3d_{3/2}$ and Ag $3d_{5/2}$ states of the Ag binding energy (Fig. 2i) [30], the bands at 87.68 and 84.07 eV were originated from the Au $4f_{5/2}$ and Au $4f_{7/2}$ states of the Au binding energy (Fig. 2j) [31], and the existence of both Au^0 and Ag^0 was also proved. Of note was that the GAA's Au and Ag binding energies had little shift compared to that of single metal Au and Ag, which fully indicated the formation of AuAg nanoalloy [32,33]. In conclusion, the results above jointly proved the GAA was well synthesized.

We explored the unique properties of GAA. As shown in Fig. 3a, the UV–vis absorbance spectra of GAA in 500 mmol/L H_2O_2, 10 mmol/L NaHS and 100 mmol/L HNO_3 were unchanged within 30 min compared with that of GAA water solution, indicative of its superior corrosion resistance and stability. As compared, the absorbance of Ag nanoparticles (NPs) decreased quickly with the addition of the above solutions even though their concentrations were one tenth of that added in GAA (Figs. S5 and S6 in Supporting information). Therefore, the encapsulation of graphitic shell facilitated the protection of AuAg nanoalloy core from various harsh environments.

We further studied the SERS effect and NIR laser mediated photothermal property of GAA. As shown in Figs. 3b–d, the SERS signals of 1 μmol/L CV, 1 μmol/L malachite green (MG) and 10 μmol/L rhodamine (R6G) boosted evidently in the presence of GAA substrate, proving its superior SERS property. The SERS spectra of these molecules recorded in the presence of GAA were consistent with their spontaneous Raman spectra, and the assignments of the major SERS bands of these molecules were exhibited in Table S1

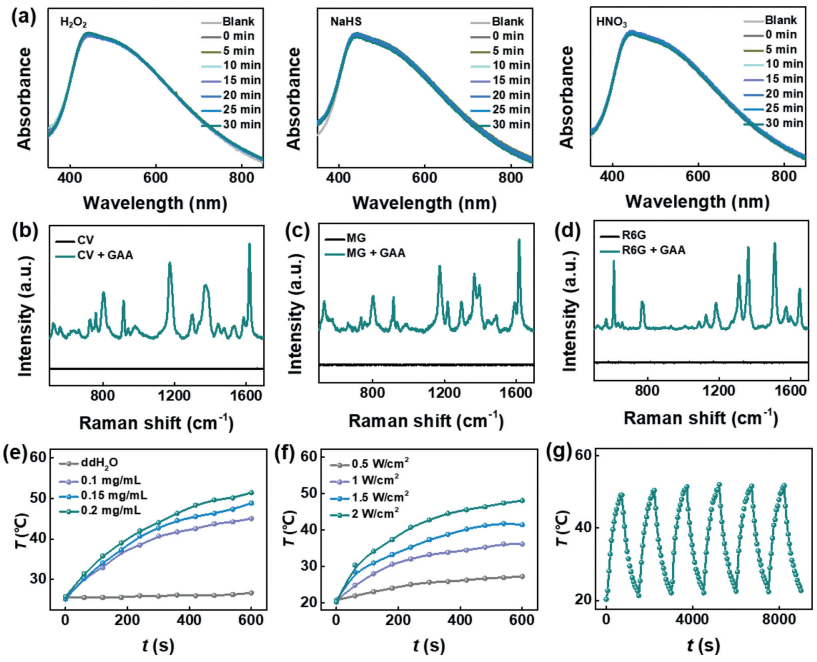

Fig. 3. Properties of GAA. (a) UV–vis absorption spectra of GAA and GAA incubated with 500 mmol/L H_2O_2, 1 mmol/L NaHS and 100 mmol/L HNO_3 for different times, respectively. SERS spectra of (b) CV, (c) MG and (d) R6G without or with the incubation of GAA under 633 nm laser excitation. (e) Heating curves of ddH_2O and diverse concentrations of GAA under the irradiation of 2 W/cm^2 808 nm laser. (f) Heating curves and (g) heating–cooling curves of 0.2 mg/mL GAA under the irradiation of different powers of 808 nm laser.

(Supporting information). As shown in Fig. 3e, double–distilled water (ddH_2O), 0.1, 0.15, and 0.2 mg/mL GAA increased by 2.8, 21.1, 24.9, and 27.5 °C, respectively, under 2 W/cm^2 808 nm laser irradiation for 10 min. Also, 0.2 mg/mL GAA under 0.5, 1, 1.5 and 2 W/cm^2 808 nm laser irradiation for 10 min increased by 7.2, 16.1, 21.4 and 28 °C, respectively (Fig. 3f). The corresponding photothermal conversion efficiency (PCE) was up to 20.73% (Fig. S7 in Supporting information). The results revealed GAA had superior NIR laser mediated photothermal property, and this property was closely related to the laser power and GAA concentration. We also proved that GAA had acceptable photothermal stability by five heating and cooling cycling tests (Fig. 3g).

CN^- and PYO are two vital biomarkers for *P. aeruginosa* infection [17,34], thus realizing their sensitive detection is of immense importance. SERS technique provides rich chemical fingerprint information and exhibits ultrahigh sensitivity, hence it shows huge potential for bioanalysis [35–40]. Herein, we used GAA solution as the SERS substrate, and quantitative analysis of CN^- and PYO as well as their simultaneous detection were inquired. It was reported that CN^- could etch noble metals including Au NPs and Ag NPs (as evidenced in Figs. S8, S9a and b in Supporting information) to form $M(CN)_2^-$ complex in oxygen–contained environments [41,42], making them unsuitable for SERS analysis of CN^-. Fortunately, GAA showed excellent stability in CN^- contained condition even the CN^- concentration was up to 1 mmol/L (Fig. 4a and Fig. S9c in Supporting information). SERS signals (~2100 cm^{-1}) [17,43] increased with the increment of CN^- concentrations (c_{CN^-}) between 50 nmol/L and 500 μmol/L (Fig. 4b), and the corresponding linear fitting curve between SERS intensities and logarithm of c_{CN^-} in Fig. 4c showing acceptable linearity. We found the SERS spectrum of PYO within 1300–1700 cm^{-1} (marked with green box) overlapped with the D and G bands of graphitic shell from GAA substrate (Fig. 4d). Hence, spectral range of 300–1000 cm^{-1} was used for SERS quantitative analysis of PYO, and the corresponding SERS spectra (~546 cm^{-1} [44,45], marked with orange box) of different PYO concentrations in the range of 50 nmol/L and 5 mmol/L were showed in Fig. 4e. A satisfactory linear fitting curve between SERS intensities and logarithm of c_{PYO} was also observed (Fig. 4f). Of note, CN^- and PYO tended to coexist in the *P. aeruginosa* infection scenario, we thus explored the simultaneous SERS detection property of GAA (Fig. 4g). As shown in Figs. 4h and i, the characteristic peaks of both CN^- and PYO were clearly observed although their concentrations were 100 times different. The results above proved the superior SERS quantitative analysis and multiplexing ability of GAA, showing broad prospects in SERS bioanalysis.

We further studied the NIR laser (2 W/cm^2 808 nm laser for 10 min) mediated photothermal antibacterial property of GAA using Gram–negative *E. coli* and Gram–positive *S. aureus* as the model *via* plate counting experiments (Fig. 5a). Both *S. aureus* and *E. coli* colony counts in the laser irradiation group had no obvious difference compared with that in control group (no GAA addition), indicating the negligible inhibitory effect of laser on the bacteria. Without the laser irradiation, the colony counts of both *S. aureus* and *E. coli* kept almost unchanged with the rising of GAA concentrations, indicating GAA had no obvious bacteriostatic activity. However, the colony counts of both *S. aureus* and *E. coli* decreased sharply as GAA concentration increased when treated with laser irradiation. Statistical analysis indicated the photothermal antibacterial efficiency of 0.1, 0.15 and 0.2 mg/mL GAA on *E. coli* were 65.2%, 97.9% and 99.6%, while that on *S. aureus* were 67.5%, 94.3% and 99.8%, respectively. Hence, ultrahigh antibacterial efficacy could be achieved using GAA as the photothermal agent under NIR laser irradiation, indicating it had potential photothermal antibacterial effect on both Gram–negative and Gram–positive bacteria.

Also, conventional live/dead bacterial viability tests were further used to study the photothermal antibacterial property of GAA. As shown in Fig. 5b, the viability of both *E. coli* and *S. aureus* irradiated with laser showed no difference compared with that in control group, while the bacterial viabilities significantly decreased with the addition of 0.2 mg/mL GAA after the laser irradiation, which further proved the satisfactory photothermal antibacterial ability of GAA. Moreover, the micromorphology of both *S. aureus*

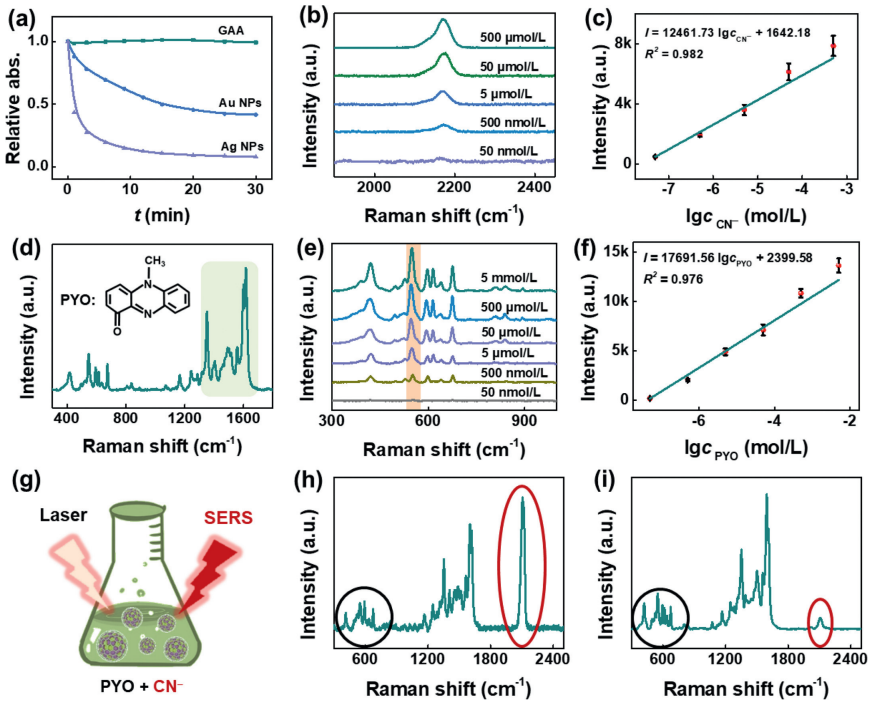

Fig. 4. GAA for SERS analysis of bacterial biomarker. (a) Relative absorbance of GAA, Au NPs and Ag NPs incubated with 1 mmol/L CN^- for different times. (b) SERS spectra of diverse concentrations of CN^- in GAA. (c) Curve fitting between SERS intensities and logarithm of CN^- concentrations. Error bars, standard deviation (SD), $n = 5$. (d) SERS spectra of PYO using GAA as the SERS substrate. (e) SERS signals of diverse concentrations of PYO in GAA. (f) Curve fitting between SERS intensities (the labeled peak in (e)) and logarithm of PYO concentrations. Error bars, SD, $n = 5$. (g) Illustration for simultaneous detection of CN^- and PYO in GAA. SERS spectra of the mixture of (h) 500 μmol/L $CN^- + 5$ μmol/L PYO and (i) 5 μmol/L $CN^- + 500$ μmol/L PYO in GAA.

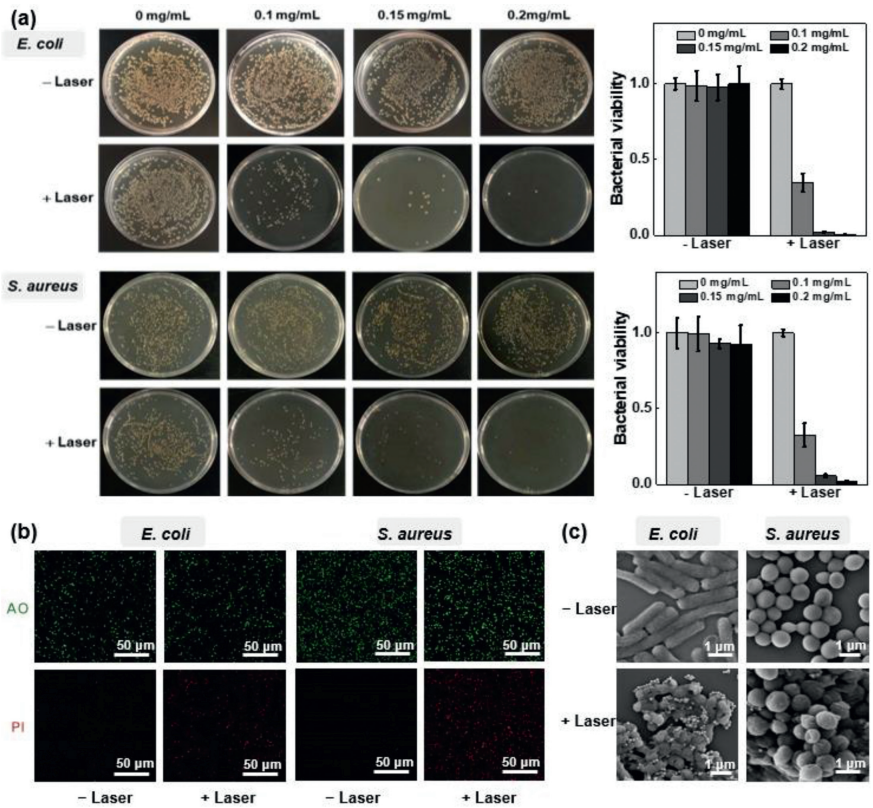

Fig. 5. GAA for photothermal antibacterial therapy *in vitro*. (a) Photos of *E. coli* and *S. aureus* colonies incubated with different concentration of GAA without or with 2 W/cm^2 808 nm laser irradiation (left) and statistical analysis of the bacterial viability (right). Error bars, SD, $n = 3$. (b) Confocal fluorescence images of bacteria without or with laser irradiation after stained with AO/PI. (c) Scanning electron microscope (SEM) images of bacteria before and after the laser irradiation.

and *E. coli* before and after photothermal antibacterial experiments were also recorded. As shown in Fig. 5c, *E. coli* and *S. aureus* exhibited smooth rods and full sphere, respectively, before photothermal treatment. However, their membranes shrank or even cracked seriously after the laser irradiation, illustrating the photothermal induced the damage of bacterial membrane. Finally, we evaluated the biocompatibility level of GAA. As shown in Fig. S10 (Supporting information), viability of C3H/10T1/2 cells kept almost unchanged with the increment of GAA concentrations up to 30 μg/mL, indicative of its superior biocompatibility. Hence, GAA could be used as a robust photothermal agent for extensive antibacterial applications.

In conclusion, ultrastable GAA with superior SERS and photothermal properties were prepared *via* the CVD method in this work, and sensitive detection of bacterial biomarkers and NIR laser mediated photothermal antibacterial therapy were achieved. Firstly, GAA with satisfactory stability and SERS property was optimized *via* rational experimental parameter control of the CVD process. Secondly, the superior stability, its SERS performance and NIR–mediated photothermal heating capacity were proved, those outstanding merits endowed it with great potential for bacterial theranostics. Next, GAA was used for SERS quantitative detection of bacterial biomarker including CN^- and PYO, and its good SERS multiplexing ability was also identified. Finally, GAA was used as the robust photothermal agent for photothermal antibacterial of both Gram–negative and Gram–positive bacteria, and ultrahigh antibacterial efficacies were achieved under NIR laser irradiation. Notably, benefiting from the good SERS and photothermal performance of ultrastable GAA, it was expected to build robust platforms for future clinical bacterial theranostics.

Declaration of competing interest

The authors declare that they have no known competing financial interests or personal relationships that could have appeared to influence the work reported in this paper.

Acknowledgments

The authors acknowledge funding support from the National Key Research and Development Program of China (Nos. 2022YFC2403501, 2020YFA0210800), National Natural Science Foundation of China (No. 22225401), Science and Technology Innovation Program of Hunan Province (No. 2020RC4017), China Postdoctoral Science Foundation (No. 2021M701145). The authors would also like to acknowledge Z. Hu and T. Yang from Shiyanjia Lab (www.shiyanjia.com) for the XRD and XPS measurements.

Supplementary materials

Supplementary material associated with this article can be found, in the online version, at doi:10.1016/j.cclet.2023.108636.

References

[1] C. Bunchorntavakul, N. Chamroonkul, D. Chavalitdhamrong, World J. Hepatol. 8 (2016) 307.
[2] C.G. Buffie, E.G. Pamer, Nat. Rev. Immunol. 13 (2013) 790–801.
[3] L. Xu, P. Deng, W. Song, et al., ACS Mater. Lett. 5 (2022) 162–171.
[4] Z. Liu, S. Li, Z. Yin, et al., Adv. Sci. 9 (2022) 2104576.
[5] Z. Yu, L. Jiang, R. Liu, et al., Chem. Eng. J. 426 (2021) 131914.
[6] W. Zhao, D. Zhang, T. Zhou, et al., Sensor. Actuat. B 350 (2022) 130879.
[7] L. Li, R. Jiang, B. Shan, et al., Nat. Commun. 13 (2022) 5249.
[8] Y. Zhao, X. Fang, M. Bai, et al., Chin. Chem. Lett. 33 (2022) 2101–2104.
[9] C. Qiu, Z. Cheng, C. Lv, et al., Chin. Chem. Lett. 32 (2021) 2369–2379.
[10] J. Huo, Q. Jia, H. Huang, et al., Chem. Soc. Rev. 50 (2021) 8762–8789.
[11] Z. Liu, X. Zhao, B. Yu, et al., ACS Nano 15 (2021) 7482–7490.
[12] N. Guo, Y. Xia, Y. Duan, et al., Chin. Chem. Lett. 34 (2022) 107542.
[13] K.M. Mayer, J.H. Hafner, Chem. Rev. 111 (2011) 3828–3857.
[14] B. Sepúlveda, P.C. Angelomé, L.M. Lechuga, et al., Nano Today 4 (2009) 244–251.
[15] A. Gutés, R. Maboudian, C. Carraro, Langmuir 28 (2012) 17846–17850.
[16] Z. Liu, L. Cheng, L. Zhang, et al., Biomaterials 35 (2014) 4099–4107.
[17] L. Zhang, J. Zhang, Z. Zheng, et al., Anal. Chem. 91 (2019) 8762–8766.
[18] M.L. Xu, L.Y. Guan, S.K. Li, et al., Chem. Commun. 55 (2019) 5359–5362.
[19] S. Li, Y. Yang, S. Wang, et al., Exploration 2 (2022) 20210223.
[20] Y. Yang, S. Li, H. Bu, et al., Front. Chem. 10 (2022) 909110.
[21] S. Wang, T. Peng, S. Li, et al., Nano Res. 15 (2022) 9327–9333.
[22] S. Li, Z. Zhu, X. Cai, et al., Chin. J. Chem. 39 (2021) 1491–1497.
[23] X. Wan, G. Long, L. Huang, et al., Adv. Mater. 23 (2011) 5342–5358.
[24] K.P. Loh, S.W. Tong, J. Wu, J. Am. Chem. Soc. 138 (2016) 1095–1102.
[25] E. Dervishi, Z. Li, F. Watanabe, et al., Chem. Commun. 27 (2009) 4061–4063.
[26] R. Siburian, H. Sihotang, S.L. Raja, et al., Orient. J. Chem. 34 (2018) 182.
[27] A. Siokou, F. Ravani, S. Karakalos, et al., Appl. Surf. Sci. 257 (2011) 9785–9790.
[28] V. Datsyuk, M. Kalyva, K. Papagelis, et al., Carbon 46 (2008) 833–840.
[29] H. Estrade–Szwarckopf, Carbon 42 (2004) 1713–1721.
[30] F. Gao, J. Lei, H. Ju, Anal. Chem. 85 (2013) 11788–11793.
[31] J.C. Yu, X.C. Wang, L. Wu, et al., Adv. Funct. Mater. 14 (2004) 1178–1183.
[32] P. Sangpour, O. Akhavan, A.Z. Moshfegh, J. Alloy. Compd. 486 (2009) 22–28.
[33] P. Sangpour, O. Akhavan, A. Moshfegh, Appl. Surf. Sci. 253 (2007) 7438–7442.
[34] R.K. Lauridsen, L.M. Sommer, H.K. Johansen, et al., Sci. Rep. 7 (2017) 45264.
[35] X. Su, X. Liu, X. Xie, et al., ACS Nano 17 (2023) 4077–4088.
[36] X. Su, X. Liu, Y. Xie, et al., Anal. Chem. 95 (2023) 3821–3829.
[37] Y. Song, D. Wang, Z. Li, et al., Chin. Chem. Lett. 33 (2022) 3879–3882.
[38] T. Xu, Y. Luo, C. Liu, et al., Anal. Chem. 92 (2020) 7816–7821.
[39] J. Li, W. Li, Y. Rao, et al., Chin. Chem. Lett. 32 (2021) 150–153.
[40] J. Li, S. Dong, J. Tong, et al., Chem. Commun. 52 (2016) 284–287.
[41] X.B. Wang, Y.L. Wang, J. Yang, et al., J. Am. Chem. Soc. 131 (2009) 16368–16370.
[42] Z. Xu, X. Chen, H.N. Kim, et al., Chem. Soc. Rev. 39 (2010) 127–137.
[43] X. Tian, Y. Liu, D. Xiao, et al., J. Power Sources 365 (2017) 320–326.
[44] I. Pastoriza-Santos, C. Kinnear, J. Pérez–Juste, et al., Nat. Rev. Mater. 3 (2018) 375–391.
[45] G. Bodelón, V. Montes-García, C. Costas, et al., ACS Nano 11 (2017) 4631–4640.